

Final Technical Report

2

Investigation of Dose Rate Dependent Electrical Activation
of Implanted Dopants in Gallium Arsenide

ONR Grant N00014-92-J-1507

AD-A277 511



Submitted by
Frederick G. Moore
Assistant Professor of Physics
Whitman College
Walla Walla, WA 99362

DTIC
ELECTE
MAR 31 1994
S F D

This document has been approved
for public release and sale; its
distribution is unlimited

2708

94-09191



94 3 23 035

Shallow Acceptor Photoluminescence (PL) Technique

The generic details of this experimental technique are widely known and reported on in the literature⁶ For this work the samples under study were held in a helium cryostat at a temperature of 10 ± 0.2 degrees Kelvin. The above-bandgap excitation was provided by either a CW diode laser operating at a wavelength of 670 nm, or by CW Ar⁺ laser operating at one of the nine major wavelengths. The excitation beam was chopped at a frequency of 100Hz and the luminescence was collected by a mirror and directed into a scanning double spectrometer. The detection of the emission was accomplished using a cooled high-purity germanium detector, and a lock-in measurement technique.

Electrical Measurements

Standard, van der Pauw geometry, Hall measurements were performed on the samples used in this study. To date two sets of measurements have been made, one at a temperature of 77K the other at room temperature. Carrier concentration and mobility information is extracted from the technique. All of the measurements were done in the low field regime.

Sample Details

All of the material used in this study was commercially obtained GaAs, produced via a Liquid Encapsulated Czochralski (LEC) technique. The material was implanted with Si²⁸ at an energy of 100 keV and a variety of doses were used to obtain atomic concentrations that fall within a range that is typical of that used for the fabrication of microelectronic devices.

The implantation procedure was followed with one of two types of annealing, either an capped (Si₃N₄) furnace anneal, or a proximity cap rapid thermal anneal. After the annealing the samples had indium contacts applied and alloyed in preparation for Hall measurement.

⁶P.J. Dean, *Prog. Crystal Growth Charact.*, 5, 89, 1982.

Results of Electrical Measurements

By way of introduction to the results of this study, please refer to fig. 1, which demonstrates the typical differentiation in carrier concentration and mobility that can arise between samples implanted at a "high" dose-rate and those implanted at a "low" dose-rate. That data shown in fig. 1 is for a set of samples that will serve as the archetype for the analysis of PL spectra. These samples are from a series that received a proximity rapid thermal anneal at 980 °C for 12 seconds.

On the horizontal axis of fig. 1 is given the dose or fluence that was used in the implantation procedure. There were a total of 12 samples in this particular set, and the data points (for sheet carrier concentration only) are labeled with the corresponding sample number. Please note that such labels could also have been added on the mobility curve but in the interest of clarity such was not done.

Note further, that there is a consistent degradation in electrical properties with dose-rate. For example, samples 1-3 and sample 8 all received the identical dose of silicon ($8 \times 10^{12} \text{ cm}^{-2}$), but the former were implanted at a "high" dose-rate (80 na/cm^2), while the latter was implanted at a significantly lower dose-rate (approximately 20 na/cm^2). At this dose (and up to a dose of approximately $1 \times 10^{14} \text{ cm}^{-2}$) the difference in carrier concentrations and mobility between the high dose-rate samples and the low dose-rate samples is comparatively minor but consistent. However, at the highest two doses the differences in carrier concentration in particular are quite dramatic. For the purposes of this report then fig. 1 should be kept firmly in mind as it demonstrates the consequences (in electrical properties) that the variation in two important implantation parameters can have.

Details of PL Technique

In this study, one important variation on the shallow acceptor PL technique was undertaken. By way of introduction to it recall that the use of an ion-beam implantation technique generates a profile of dopant within the sample (and consequently a carrier concentration profile). This profile has a gaussian shape, that is the concentration of silicon beneath the surface of the sample can be described as:

$$N(x) = \frac{\emptyset}{k\sigma} \exp\left(-\frac{(x-R)^2}{2\sigma^2}\right)$$

Where the dimensions of $N(x)$ are atoms per cm^3 , k is a numerical constant, \emptyset is the implantation dose of fluence and R and σ are parameters that are governed by the implantation energy (in this case 100 keV), and the distance beneath the surface of the sample is given by x .

After implantation and annealing the carrier concentration can-to a first approximation-be thought to vary with depth in the same fashion as the atomic concentration of the dopant. Since most standard PL techniques assume a constant concentration of carriers (with respect to depth beneath the surface of the sample) there is not an agreed-upon method to analyze PL spectra from implanted samples.

In an effort to address this difficulty we have undertaken a series of PL spectra from each sample using a variety of excitation wavelengths. The penetration depth of above band-gap light into a semiconductor varies (longer wavelengths have a longer penetration depth, the converse being true as well). Using this fact we have chosen a set of excitation wavelengths whose penetration depth ranges from approximately 3000\AA (670 nm) to less than 1000\AA (457.9 nm).

Since the intensity of the excitation beam is attenuated beneath the surface of the sample at different rates, it is possible to effectively probe different regions of the samples by utilizing different excitation wavelengths. For the purposes of this report we will discuss results from three excitation wavelengths: 670 nm, 514.5 nm and 488 nm. In terms of the gaussian profiles discussed above, these three wavelengths can be thought to probe regions of the sample: well beyond the peak of the gaussian profile (670 nm), to approximately the peak of the profile (514.5 nm), and the near-surface edge of the profile (488 nm).

The power densities of the different excitation wavelengths were kept well below the PL saturation level and the power densities at the different excitation wavelengths were adjusted to maintain a constant photon-flux.

Raw PL Data

The data presented in fig. 2 through fig. 6 are pairwise comparisons (between high dose-rate and low dose-rate) of samples that received the identical dose of silicon. Each page contains three plots which are labeled with the excitation wavelength that was used. The vertical scales on all of the data are relative intensities (in arbitrary units). While the absolute scale may be shifted from plot to plot, within a single graphic (for example fig. 3, 488nm excitation) the scales used for the two different sample's spectra are the same. Hence for the aforementioned spectra it is clear that the integrated PL intensity for Sample #2 (high dose-rate) is significantly higher than for sample #8 (low dose-rate).

One quite interesting feature of this data can be seen in fig. 4 through fig. 6. These figures pertain to the most highly doped of the materials (with silicon doses of $1 \times 10^{14} \text{ cm}^{-2}$ and above). Please note that the main features of these spectra show a distinct shift between the high dose-rate samples and the low dose-rate samples, with the latter consistently being shifted to lower energy.

At this stage it is clear that the analysis of these data will be significantly more complicated than is typically undertaken in the literature. To date, most shallow acceptor PL studies have made use of the technique almost in a survey fashion—to identify the presence (or absence) of a particular species of acceptor. Unfortunately, as P.J. Dean discussed in reference 2, at higher doping levels there are several competing mechanisms at work in GaAs which make an unambiguous determination of acceptor species difficult.

Certainly this is the case in the current study. At technologically important doping levels the carrier concentration is high enough to cause both shifts in the expected transition energies along with broadening of the transitions. In the raw data attached (for example in fig. 2) it is likely that the large central feature arises as a result of transitions occurring between several electronic levels—and while there are some qualitative comparisons to be made between low and high dose-rate materials few quantitative conclusions can be drawn.

To provide a more rigorous basis from which to analyze this raw data we have resorted to an elaborate lineshape fitting approach.

Lineshape Fitting

The basis of this work was taken from a report in the literature by workers at the University of Texas, Dallas who used a simplex algorithm to provide for lineshape analysis of data from electro-reflectance measurements made on GaAs materials⁷. The inputs to this algorithm are the transition energies which are expected to account for the spectra and the lineshape type (either gaussian or lorentzian—so far we have restricted our analysis to these pure lineshapes not allowing for mixing between them). Our starting point then, for this work is the determination of the specific transitions and their transition energies that are to be expected. A careful perusal of the literature suggests that there are two acceptor species which could be expected in the samples that are part of this study.

Since carbon is a shallow acceptor present in moderate concentrations in LEC grown GaAs (C_{As}) it is only prudent to expect its presence. The only other acceptor which could reasonably be expected in these materials is the shallow silicon acceptor which results from a silicon atom resident on the arsenic sublattice (Si_{As}). The literature is replete with observations of these shallow acceptor and the observed energies are well known⁸. For a free-to-bound (FB) transition from the conduction band to a C_{As} the transition energy is 1.4850 eV. For the FB transition to a Si_{As} the energy is 1.4935 eV. The uncertainties in these energies is given by the cited author as being ± 0.3 meV

Two additional complications need to be considered before proceeding. First, given the relatively high concentrations of dopant in these samples it is reasonable to expect to see donor-acceptor (DAP) transitions in the PL spectra. Donor levels in GaAs are known to be 0.0058 eV below the conduction band, and since in the present case there are two acceptors to consider this gives rise to another pair of transition energies. The energies of these transitions then are $(1.4850 - 0.0058)$ eV = 1.4792 eV, and also $(1.4935 - 0.0058)$ eV = 1.4877 eV.

The following notation will be used in subsequent discussion:

Transition	Energy	Notation
band to C_{As}	1.4850	C_{FB}
band to Si_{As}	1.4935	Si_{FB}
donor to C_{As}	1.4792	C_{DAP}
donor to Si_{As}	1.4877	Si_{DAP}

⁷J.P. Estrera, W.M. Duncan and S.R. Slaughter, *Computers in Physics*, 6, p. 360, 1992.

⁸D.J. Ashen, P.J. Dean, D.T.J. Hurle, H.B. Mullin and A.M. White, *J. Phys. Chem Solids*, 36, 1041 1975.

The other input to the fitting procedure is the lineshape, either gaussian:

7

$$I = \frac{A_0}{\sqrt{2\pi}\Gamma} \exp\left(-\frac{(E - X_0)^2}{2\Gamma^2}\right)$$

or lorentzian:

$$I = \frac{A_0}{(\Gamma^2 + (X_0 - E)^2)}$$

In both of these expressions A_0 is the amplitude, Γ is the width of the line and X_0 is the location, in energy, of the position of the line. The fitting algorithm then allows for the total spectrum to be the sum of several individual lines.

The presence of a fifth transition, in addition to the four which are discussed on the previous page, is a concession made with a nod to the most intractable complexity in this study. As one can see by perusing the raw data contained in figs. 2-6 the systematic creation of higher silicon doping levels in the GaAs material results in a consistently growing "low energy" background in the PL spectra. This phenomena is particularly noticeable in the lower wavelength excitations beginning with samples 5 and 10.

After a lengthy review of the literature and discussions with colleagues at the Naval Research Laboratory, we are persuaded by the conventional wisdom that this low energy "feature" is a result of a systematic destruction of the crystalline quality of the samples as a result of physical damage occurring during the implantation process. This conventional wisdom must be combined with the knowledge that (in these more highly doped samples) the carrier concentration at the peak of the implantation profile generates a degenerate conduction band in the material. Together these conditions represent a difficult problem for our analysis.

In order to continue and generate a consistent analysis the following strategy was employed. The 488nm excitation probes the region of the sample that is both the most highly damaged (recall that the greatest implantation damage occurs just before the median end-of-range of the implanted ion) and that which contains the highest doping levels. Consequently, it is reasonable to expect that the electronic transitions which result in the low energy feature occur primarily in this shallow region of the sample. By determining the energy at which this feature is centered, we may attempt to account for its presence by including in the formal lineshape fitting procedure a broad low energy transition centered at this same position. So then, for each sample the position of this low energy transition is obtained by altering the lineshape fitting routine so as to allow it to obtain the best fit possible on the low energy side of the main central feature.

With this position determined then, the fitting routine is given the positions of the four acceptor-related transitions plus the position of the low energy background. The routine is then set so it will not alter the position, in energy, of these lines and the algorithm is allowed to proceed to a least-error "best fit" to the actual spectral data. It is this procedure then that generates results as good as that shown in fig. 7a and fig. 7b.

We now have at our disposal a systematic means to simplify the complicated spectral features which result free-to-bound and donor-acceptor luminescence. Using the integrated intensities of the four separate lines, which are present in each sample, we can begin comparing the relative intensities of these transitions across the sample matrix and then correlate this information to the actual carrier concentrations.

Integrated Intensities from Lineshape Fits

Using the technique described in the previous section we have accomplished fits for the samples which are shown in fig. 1. The information which results from this process is a collection of linewidths and amplitudes for the transitions: C_{FB} , Si_{FB} , C_{DAP} , S_{DAP} . With this information the integrated intensity for each of the transitions can easily be determined. Performing this task results in a set of four integrated intensity values for each of the previously mentioned transitions for each excitation wavelength.

Analysis of Integrated Intensities

Shown in fig. 8 through fig. 12 are the fractional integrated PL intensities for the samples that are depicted in fig. 1. The fractional intensities are calculated by determining the absolute integrated intensity for each of the four transitions, for each excitation wavelength. A total integrated intensity is obtained by adding these four values together and then the fractional contribution to the total intensity is calculated for each transition. For example in fig. 8 the bottom-most sample is denoted "F234#1, 670". This label refers to sample #1 in fig. 1, which received a $5 \times 10^{12} \text{ cm}^{-2}$ implant of silicon at our standard high dose-rate. When measured and analyzed in accordance with the procedures described herein the PL emission from the sample is ascribed in the following manner: roughly 18% from C_{FB} transitions, 24% from C_{DAP} transitions, 33% from Si_{FB} , and 25% from S_{DAP} .

Further, within a single figure the corresponding high dose-rate and low dose-rate samples are compared, and the excitation wavelength dependence is also given. Clearly fig. 8 through fig. 12 contain a large amount of information.

Our analysis to date has not differentiated between the details of the S_{IFB} versus S_{IDAP} luminescence or the C_{FB} versus C_{DAP} luminescence. Instead we have taken as our initial measure the fraction of the total PL intensity that is related to silicon acceptors. This value is calculated by simply adding together the fractional intensities for the S_{IFB} and for the S_{DAP} transitions. Recall that the presence of either of these transitions is an indication of silicon residing on the arsenic sublattice, which we have postulated is related to the dose-rate used to perform the implantation.

In fig. 13 through fig. 15 is shown the fraction of PL intensity that is related to silicon impurities. Within each figure the entire fluence range is given and the pairwise low versus high dose-rate samples are shown. Across the three figures the experimental parameter being varied is the excitation wavelength.

For fig. 13 (670 nm excitation) an interesting trend is observed. Beginning at the lowest fluence samples, the low dose-rate samples show consistently less silicon related PL intensity than the corresponding high dose-rate samples. This trend continues to higher fluences, but does not carry through to the highest fluence. The pairs of samples which do show this trend support the hypothesis that it is a dose-rate dependent occupancy of the arsenic lattice by silicon that is behind electrical properties that were discussed earlier in this report.

In fig. 14 and fig. 15 a similar trend is absent. These excitation wavelengths used in these two figures probe the near-surface regions of the samples which include the most highly doped regions of the implantation profile. Consequently, it is not surprising to note that for both fig. 14 (514.5 nm excitation) and fig. 15 (488 nm excitation) the fraction of the PL intensity from silicon-related transitions is significantly higher than for the 670 nm excitation which is given in fig. 13.

For this latter instance note that all samples are below the 60% level and most are below the 50% level. Whereas for the other two excitation wavelengths all but three samples show a PL silicon fraction above 50% and most are significantly above 50%, some approaching 80%. While the majority of the fluence paired samples do show the low dose-rate member to have a smaller fraction of its PL intensity to be silicon-related there is no consistent trend.

The Direction of Further Analysis

While there is some confirmation of our original hypothesis in the results discussed herein some significant issues remain. Notable among these unresolved issues is the lack of a consistent trend (as discussed in the discussion above) in data from the shorter wavelength excitation experiments.

By way of starting towards the next stage of analysis of our results please note that to this point we have examined the data from the PL experiments on the basis of silicon fluence used during the implantation procedure. This method was the most straightforward means by which we could attempt to relate the electrical properties of the implanted samples to their optical properties. As is evident from fig. 1, an increase in the implantation fluence does indeed result in increased carrier concentrations for all but a single sample. A better means by which to make the relevant comparisons would be to consider the actual carrier concentrations. However, since the two quantities (silicon fluence and carrier concentration) track each other except for a single sample it is unlikely that this method would prove satisfactory.

A more promising avenue of thought is to consider the incremental increase in carrier concentration with increased silicon fluence: $\frac{\Delta N}{\Delta \Phi}$. For example in fig. 1 the samples in the range of fluence between $5 \times 10^{12} \text{ cm}^{-2}$ and $8 \times 10^{13} \text{ cm}^{-2}$ show a consistent increase in carrier concentration with fluence, whereas at fluences above $8 \times 10^{13} \text{ cm}^{-2}$ the situation is clearly changed. Indeed for the higher fluence, high dose-rate samples there is actually a decrease in carrier concentration with increased fluence.

As a strategy then, we are hopeful that a comparison between $\frac{\Delta N}{\Delta \Phi}$ and the results of our PL experiments will yield a more unambiguous confirmation of our original hypothesis.

Figure Captions

- Fig. 1** Shown in this figure are the measured Hall sheet carrier concentrations (N) measured on samples that had been implanted at the indicated fluence (\emptyset) of silicon dopant. Also indicated are the Hall carrier mobilities (μ) of the samples. Note that each implantation fluence was accomplished at a high dose-rate and a low dose-rate and that this implantation parameter has a strong effect on the electrical properties of the samples. Note too, that each sample fluence/dose-rate combination has been assigned a numerical designation for future reference.
- Fig. 2 through Fig. 6** These figures show the raw PL data which was used in this analysis. Each figure represents a pairing of samples (identical dose, different dose-rate) which has been measured at the indicated excitation wavelengths. The horizontal axis is the energy of the PL emission, while the vertical axis is PL intensity in arbitrary units.
- Fig. 7a,7b** In these two graphics we show the success that our lineshape fitting routine can accomplish. In fig. 7a is a PL spectra that is typical of the results of our study. Along with this experimental data (Data Curve) is plotted our best lineshape fit to the data. The process is typically so successful that if it were not for the markers-in this case "x"-it would be impossible to resolve the two curves.
- In fig. 7b, the experimental data is again shown but this time the individual five lineshapes which have been fit to the data are plotted.
- Fig. 8 through Fig. 12** In these five graphics the integrated fractional intensities of the four transitions which we are attempting to fit are plotted. In each graphic the two lined regions represent the two different carbon related transitions that we consider, while the two greyscale regions represent silicon related emission. Each figure represents a single silicon fluence (\emptyset) and shows each of the three excitation wavelengths used at each fluence and at each dose-rate.
- Fig. 13 through Fig. 15** In these three figures the integrated fractional intensities for the silicon related emission only. Each figure represents data from a different excitation wavelength experiment and the low dose-rate/high dose-rate samples are show adjacent to each other.

Fig. #1

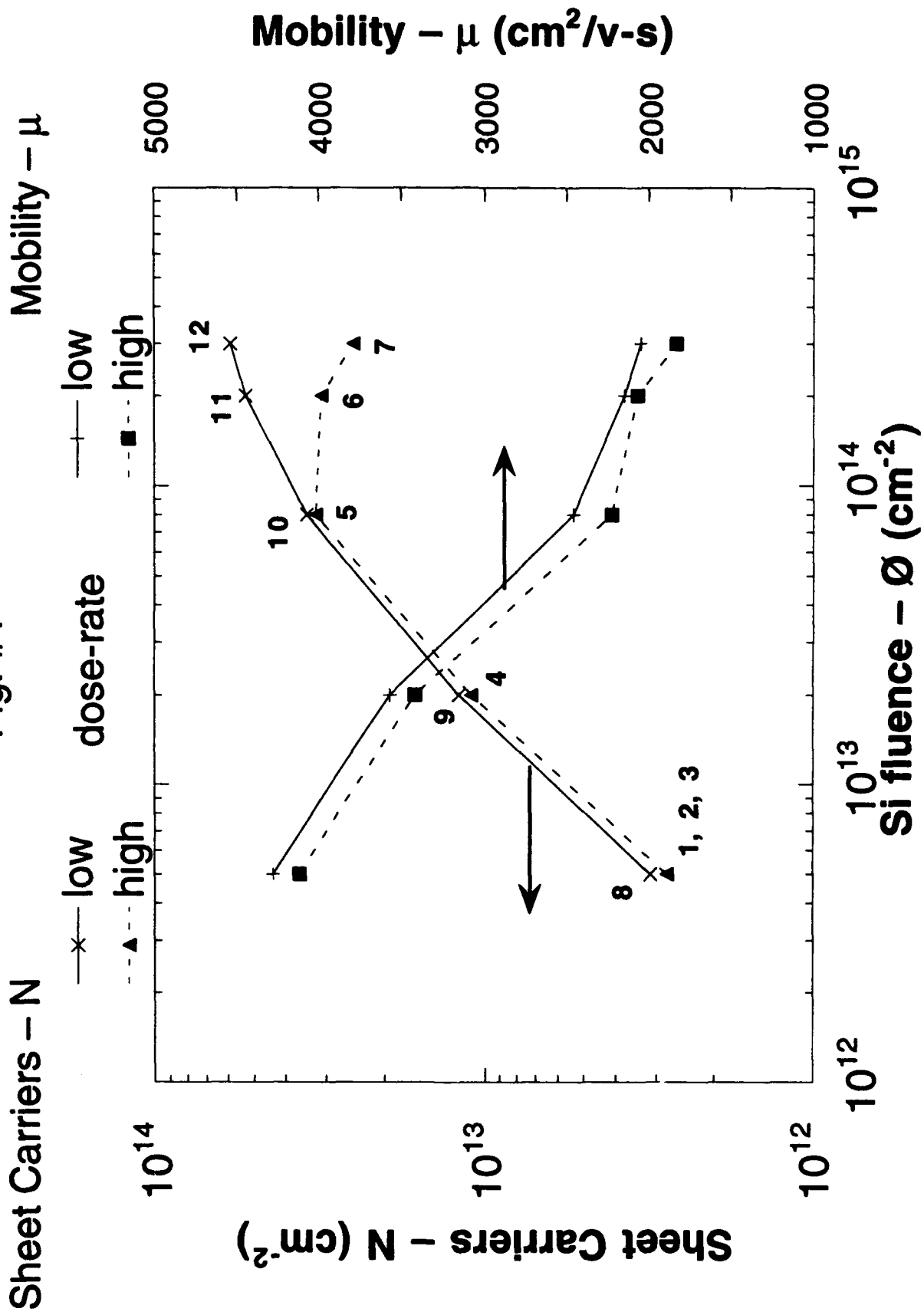
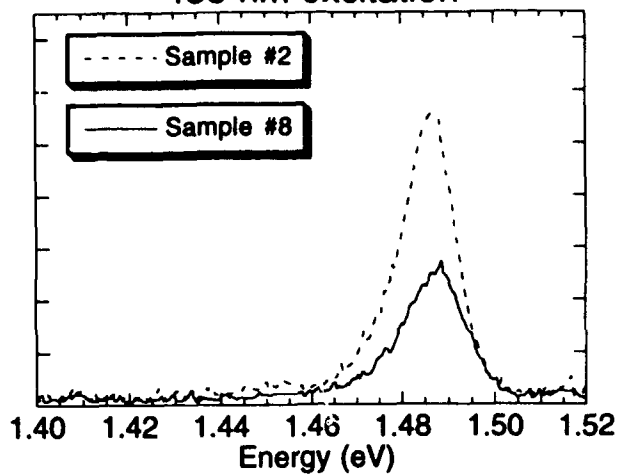
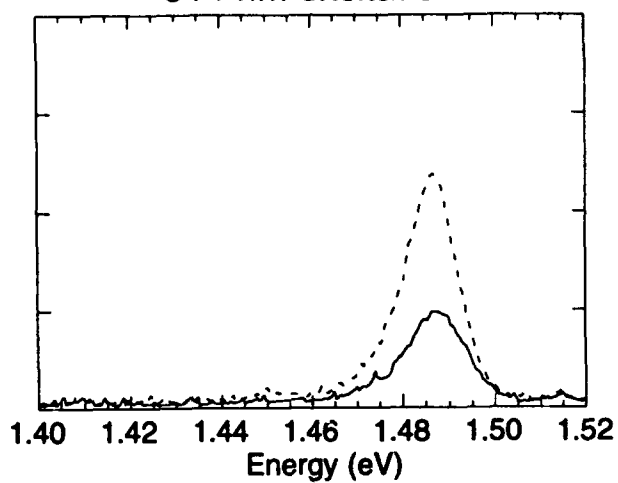


Fig. #2

488 nm excitation



514 nm excitation



670 nm excitation

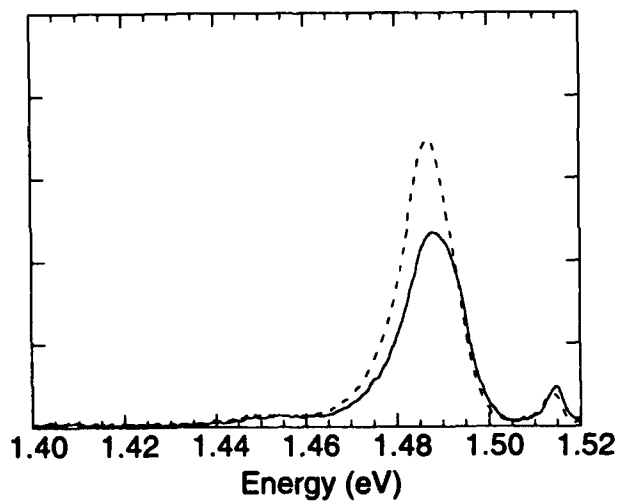
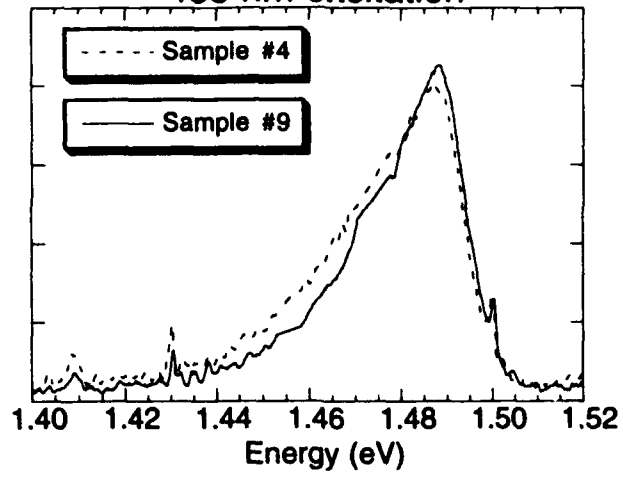
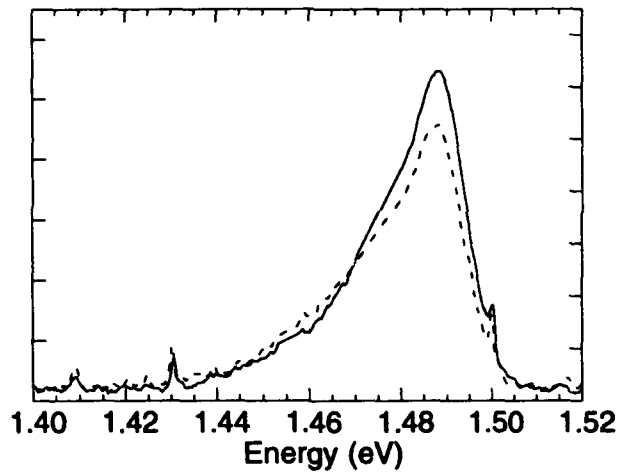


Fig. #3

488 nm excitation



514 nm excitation



670 nm excitation

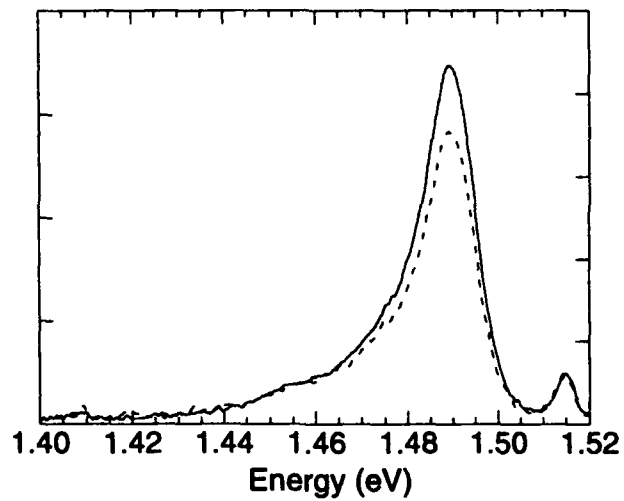


Fig. #4

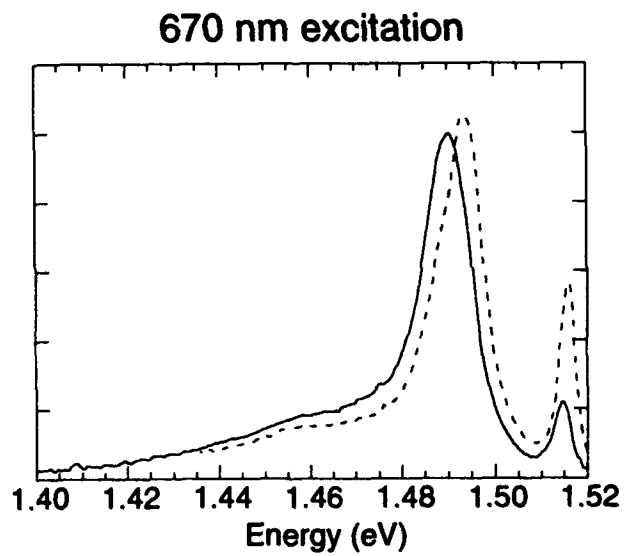
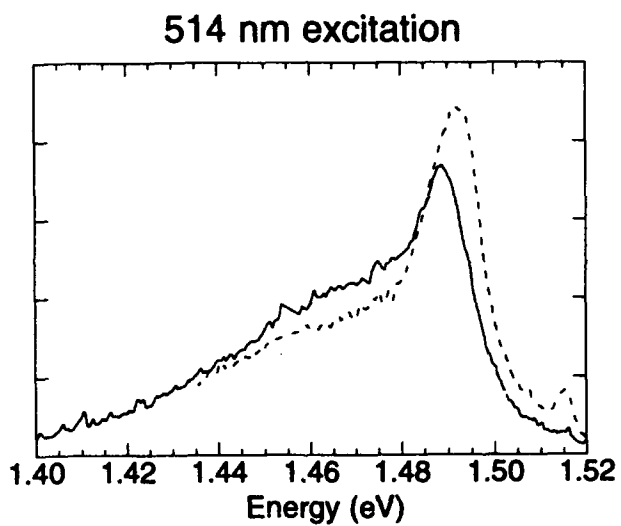
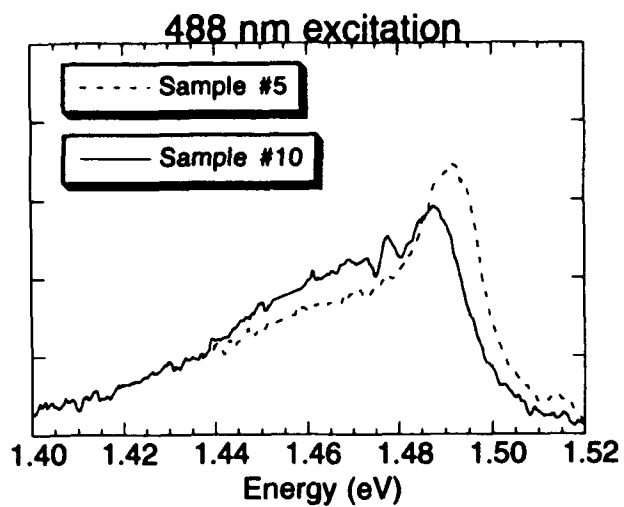


Fig. #5

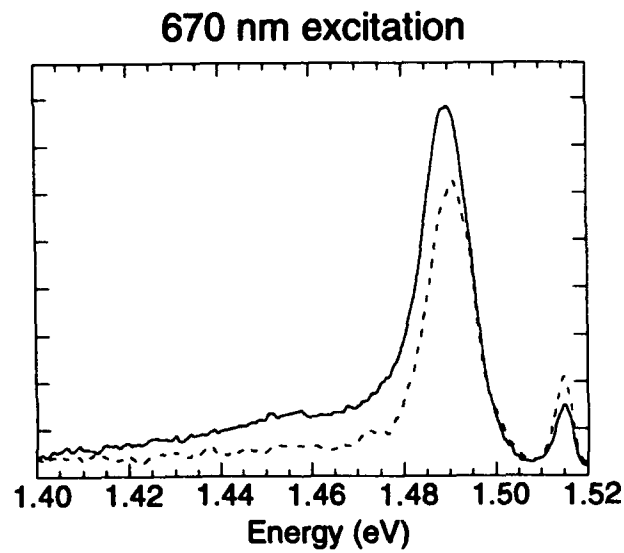
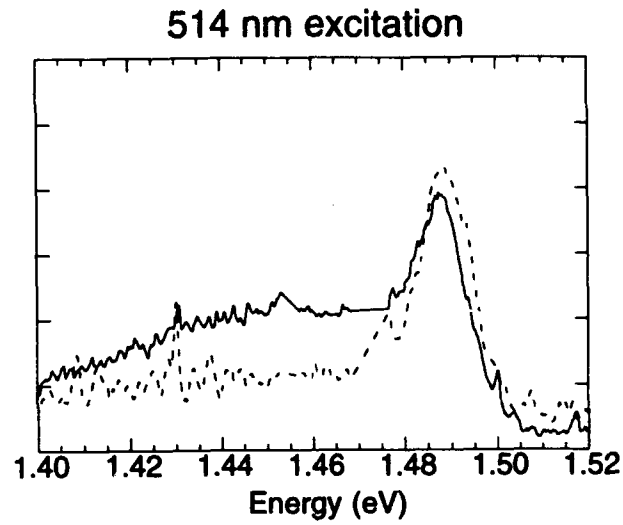
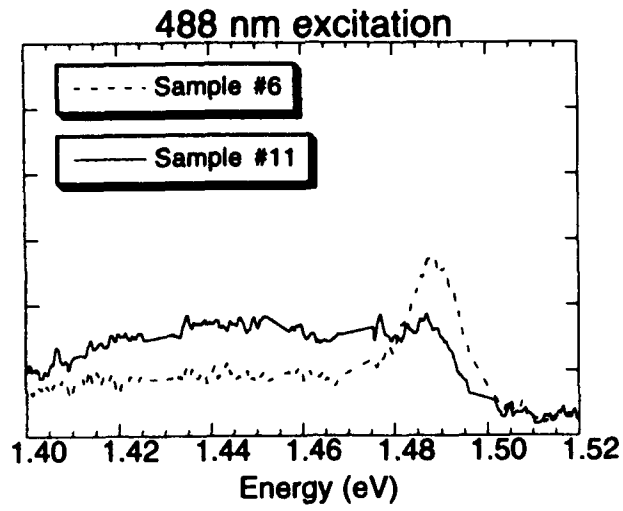


Fig. #6

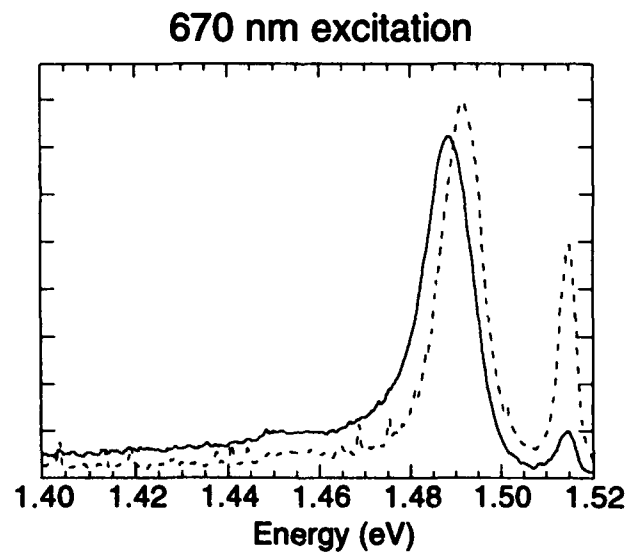
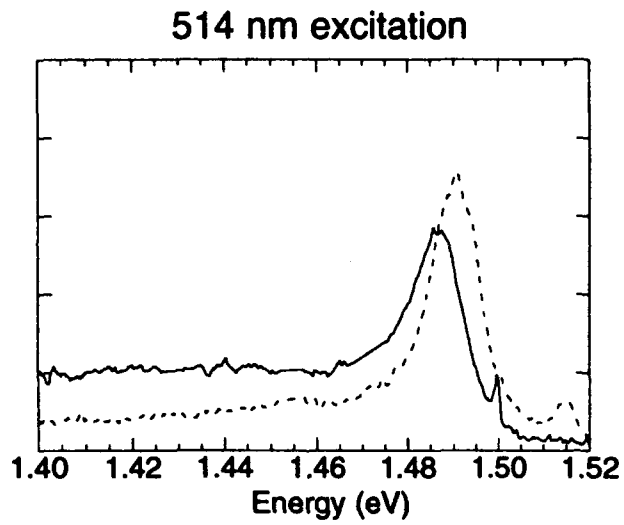
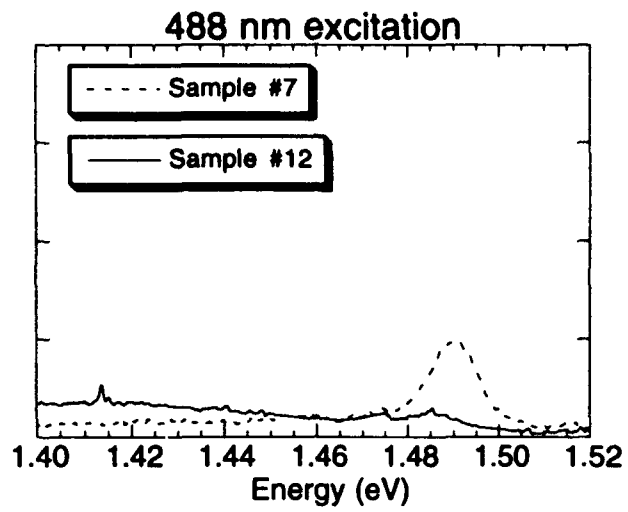


Fig. #7a

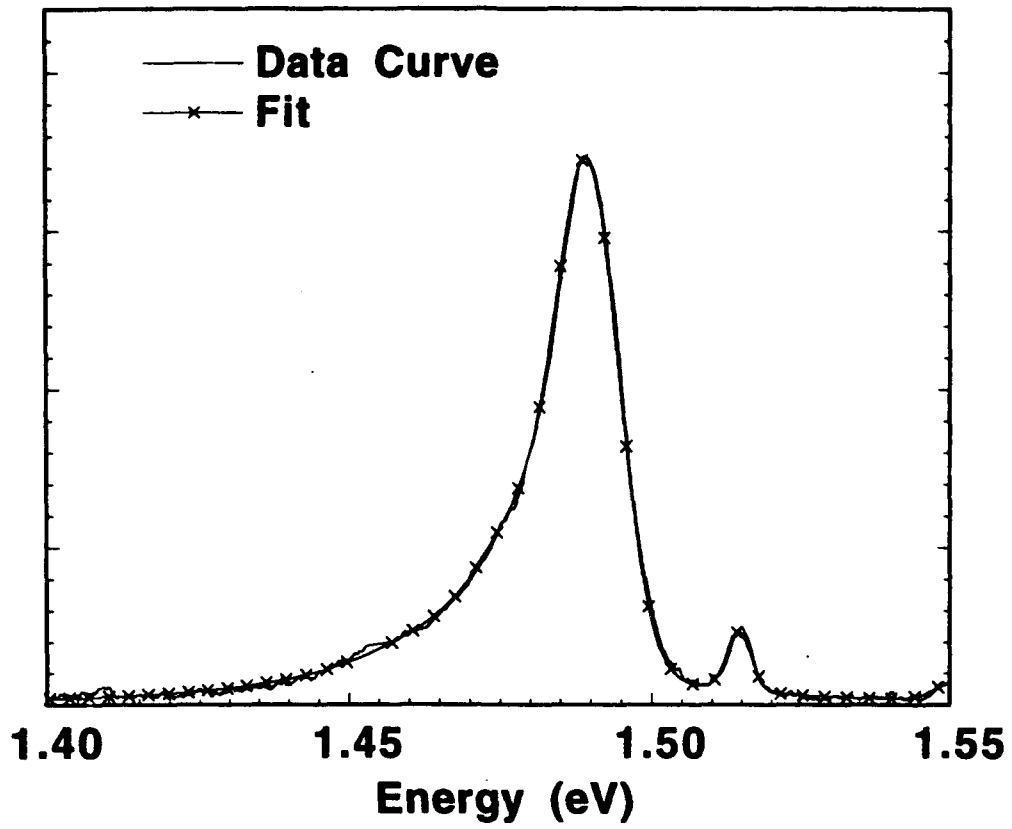


Fig. #7b

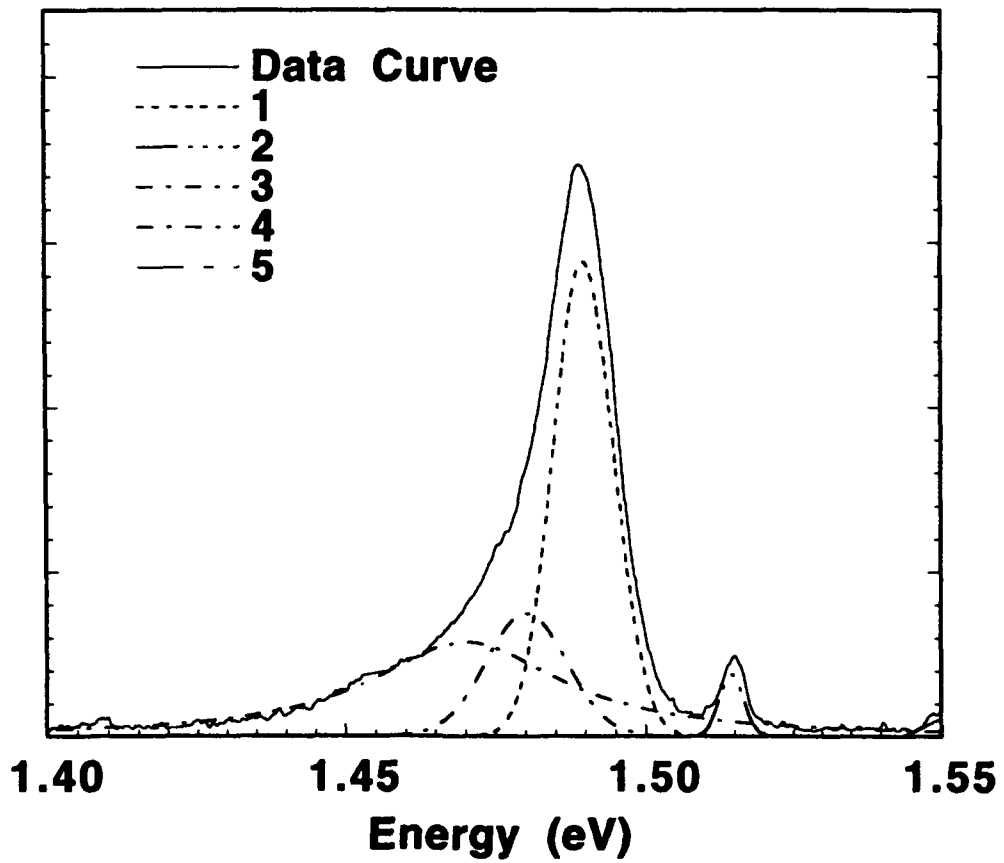


Fig. #8

$\Phi = 5 \times 10^{12} \text{ cm}^{-2}$

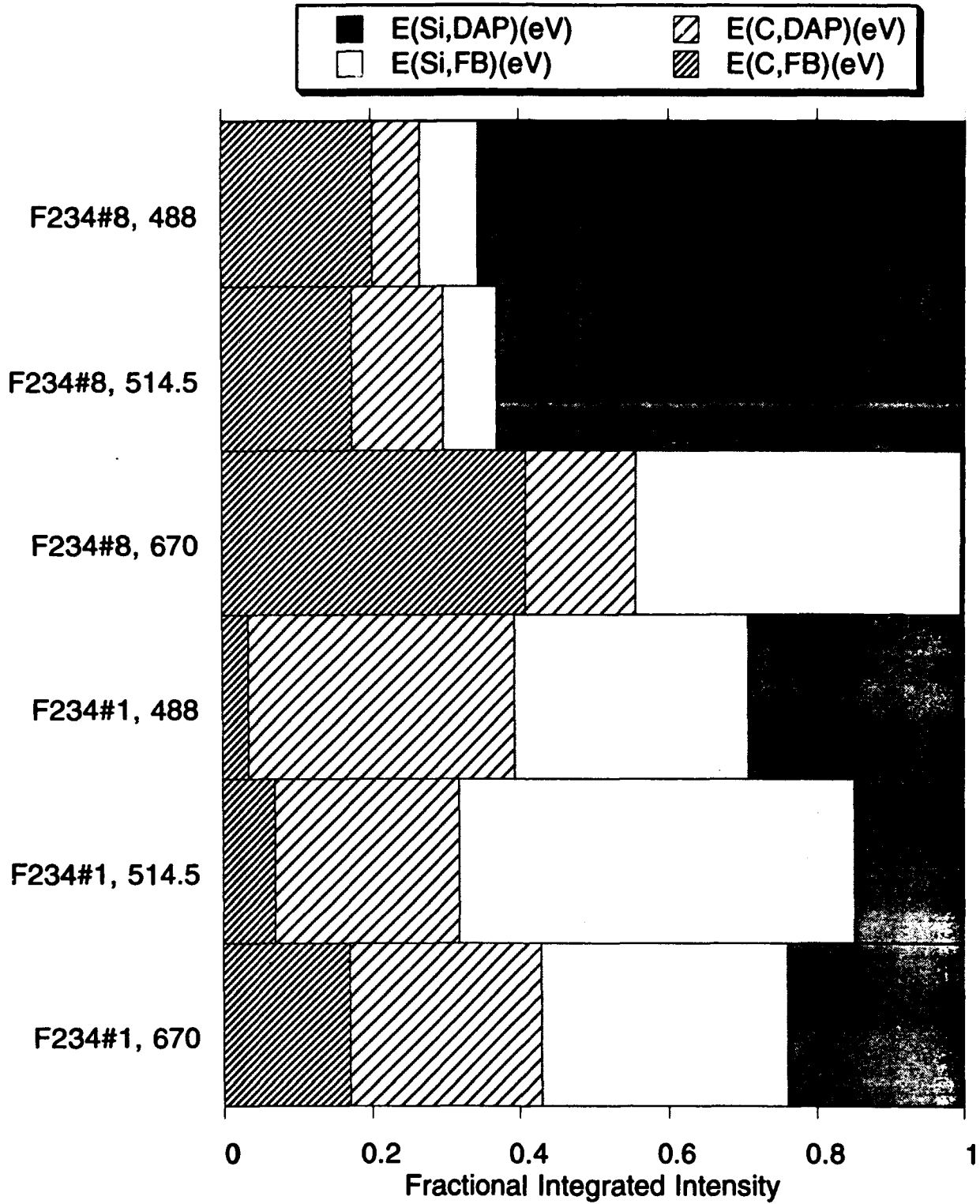


Fig. #9

$\emptyset = 2 \times 10^{13} \text{ cm}^{-2}$

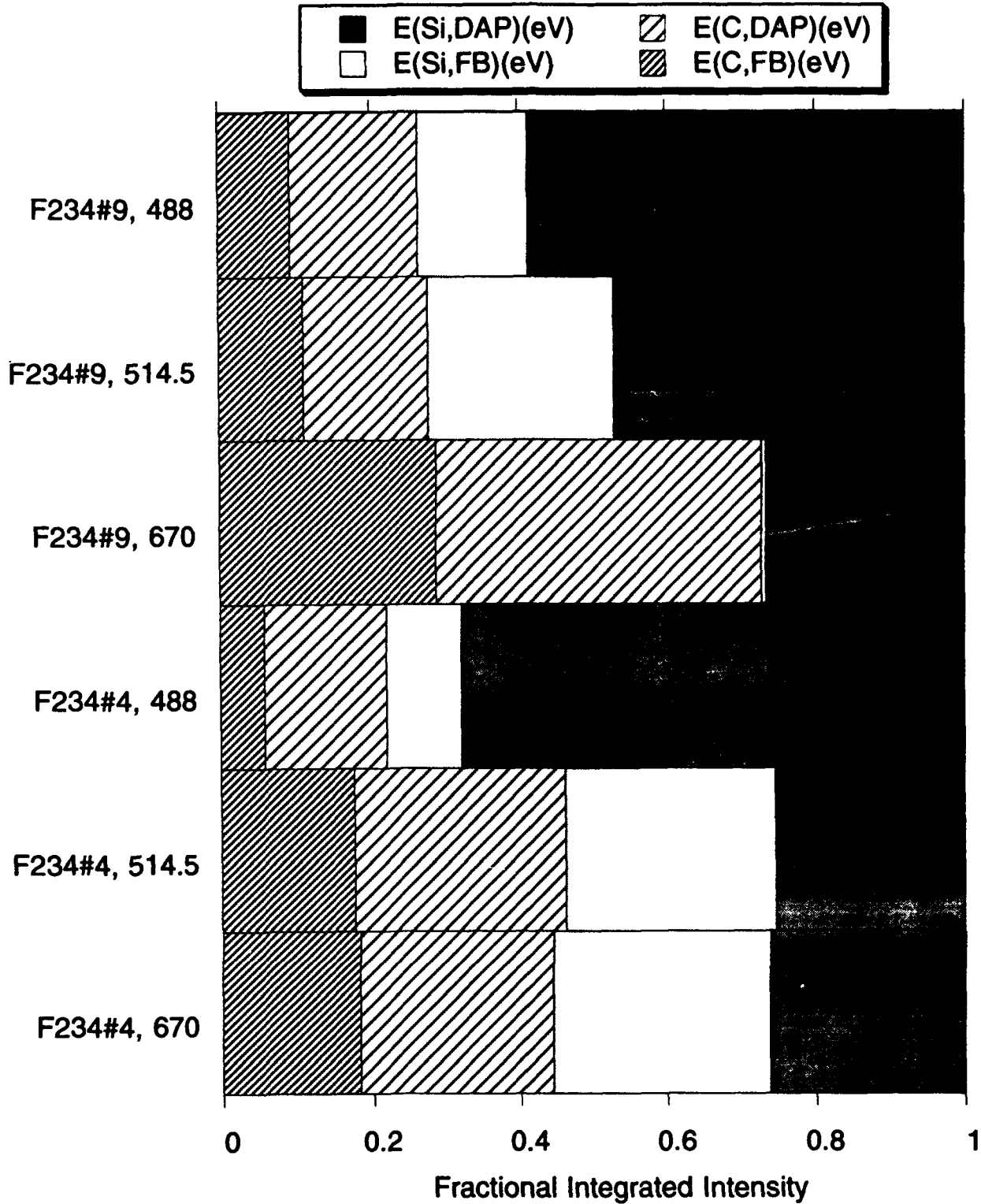


Fig. #10

$\emptyset = 1 \times 10^{14} \text{ cm}^{-2}$

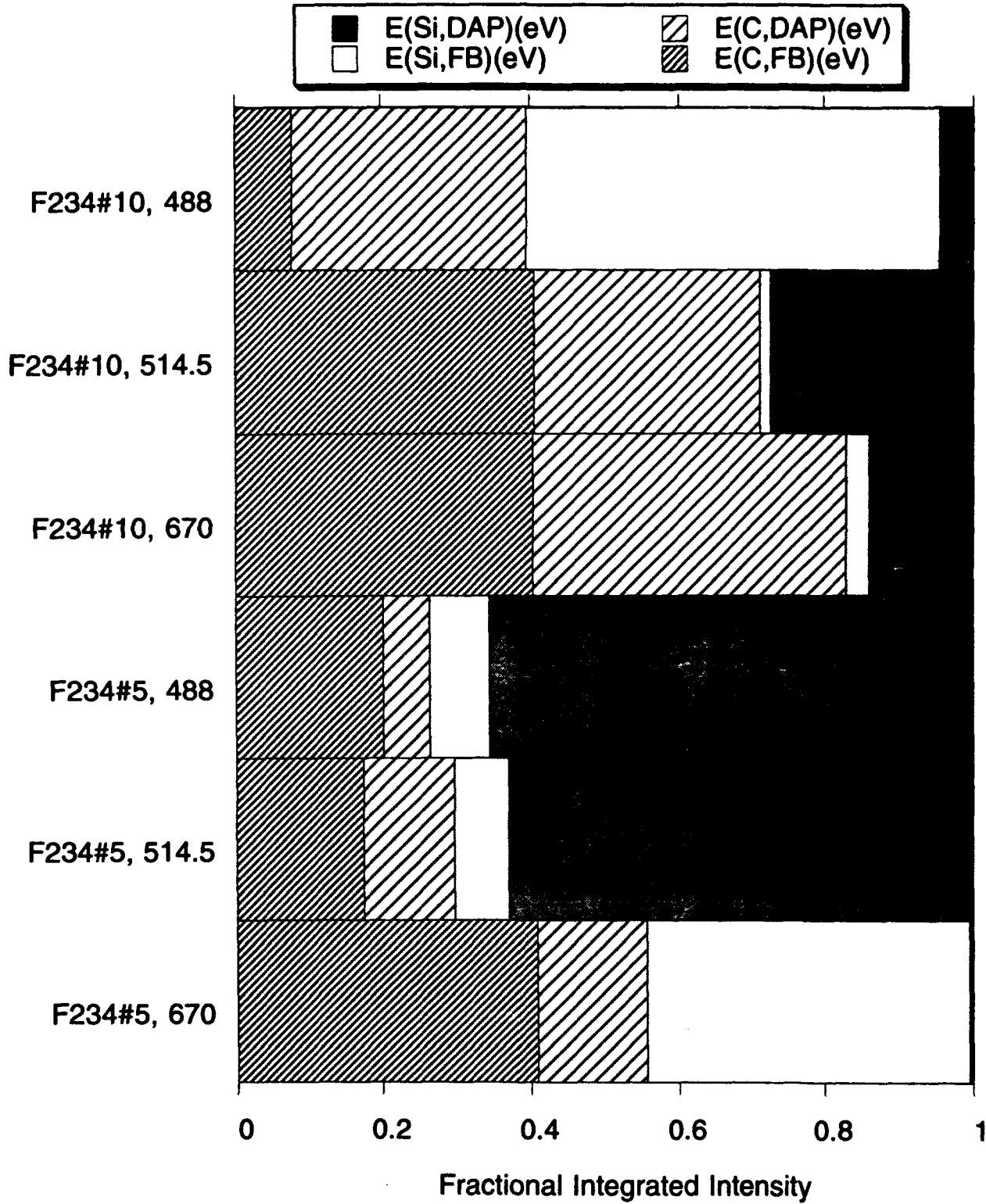


Fig. #11

$\emptyset = 2 \times 10^{14} \text{ cm}^{-2}$

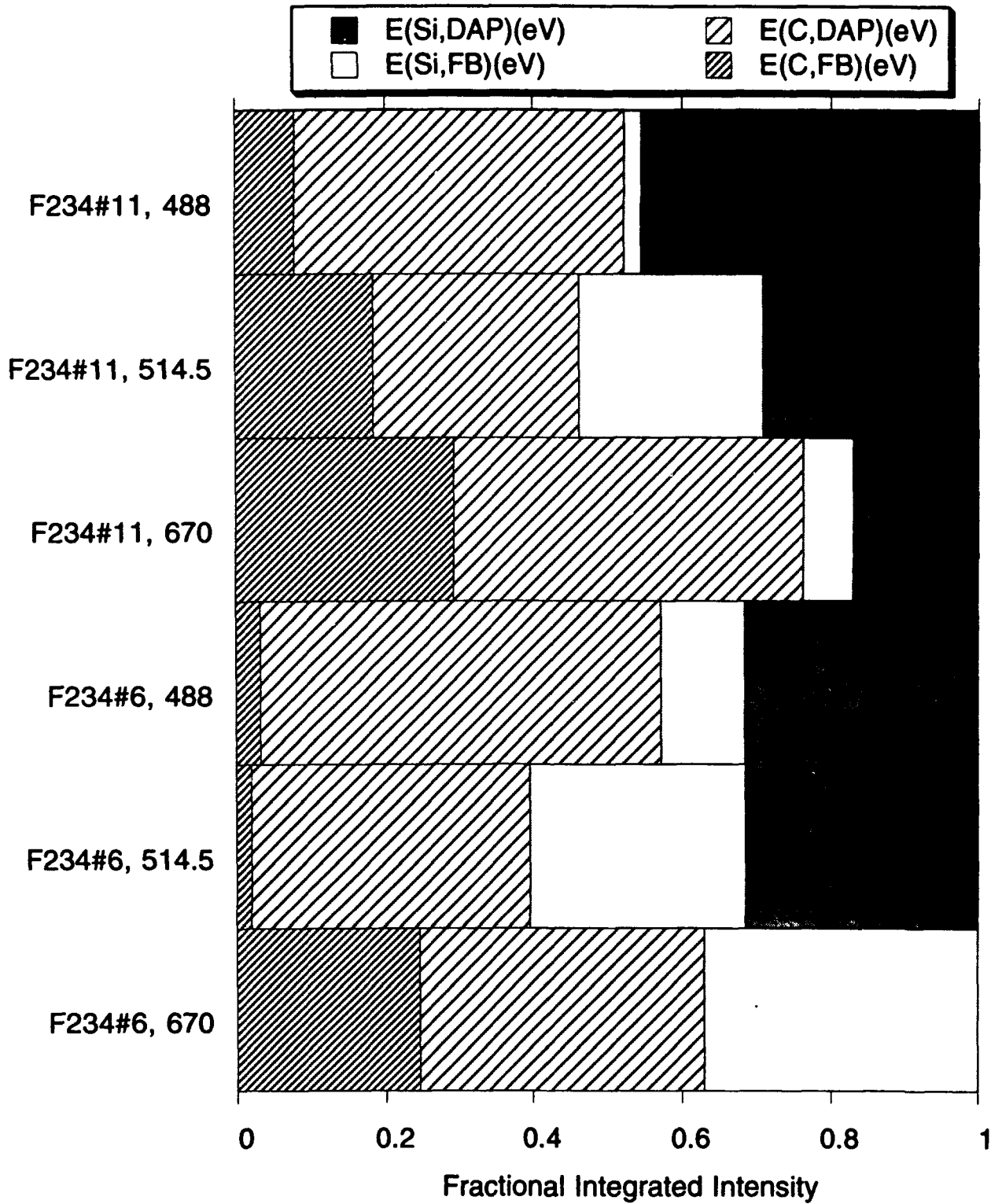


Fig. #12

$\Phi = 3 \times 10^{14} \text{ cm}^{-2}$

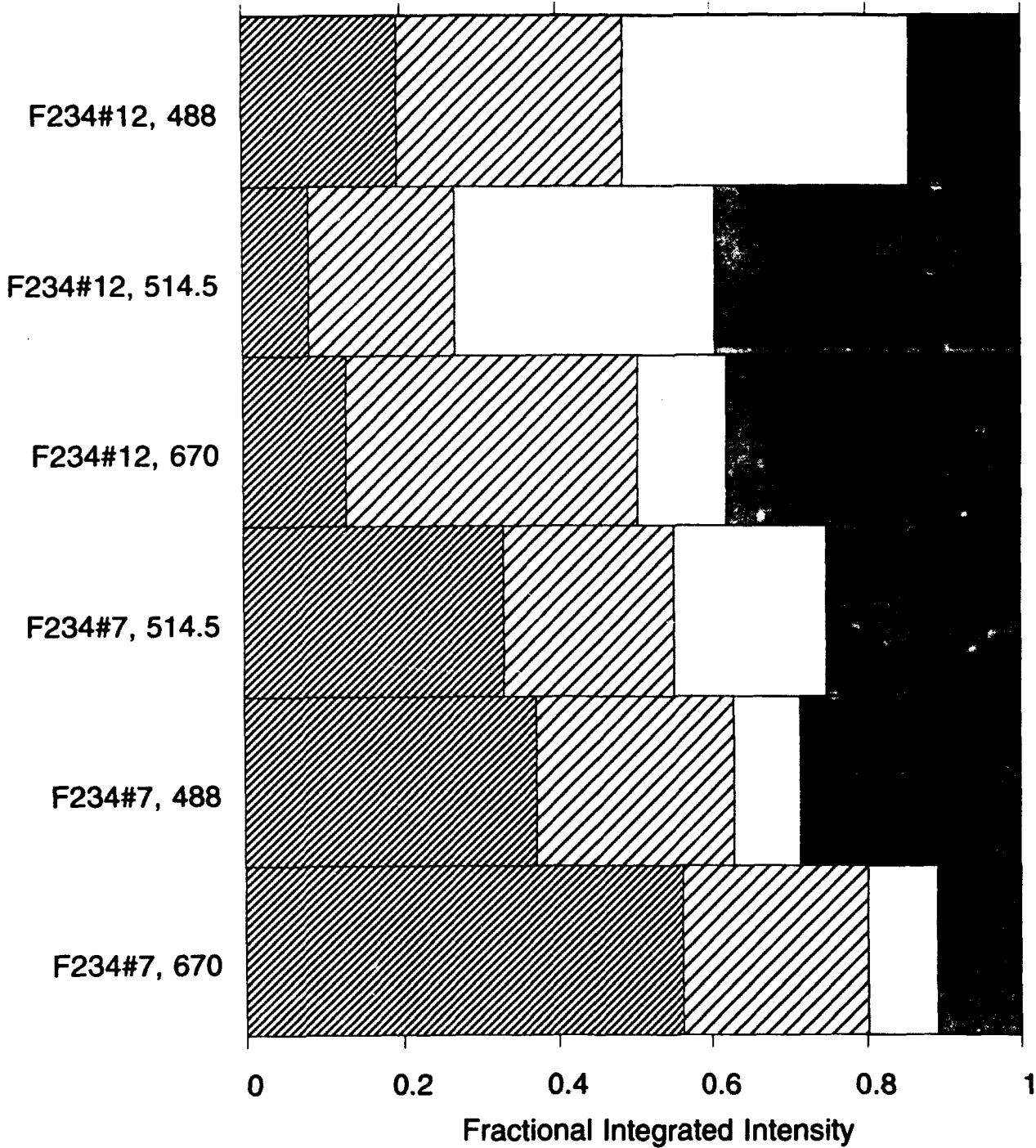
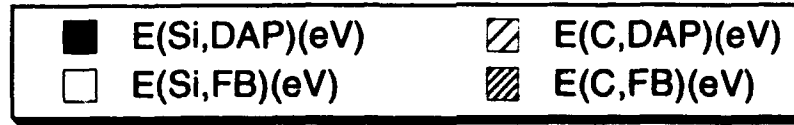


Fig. #13

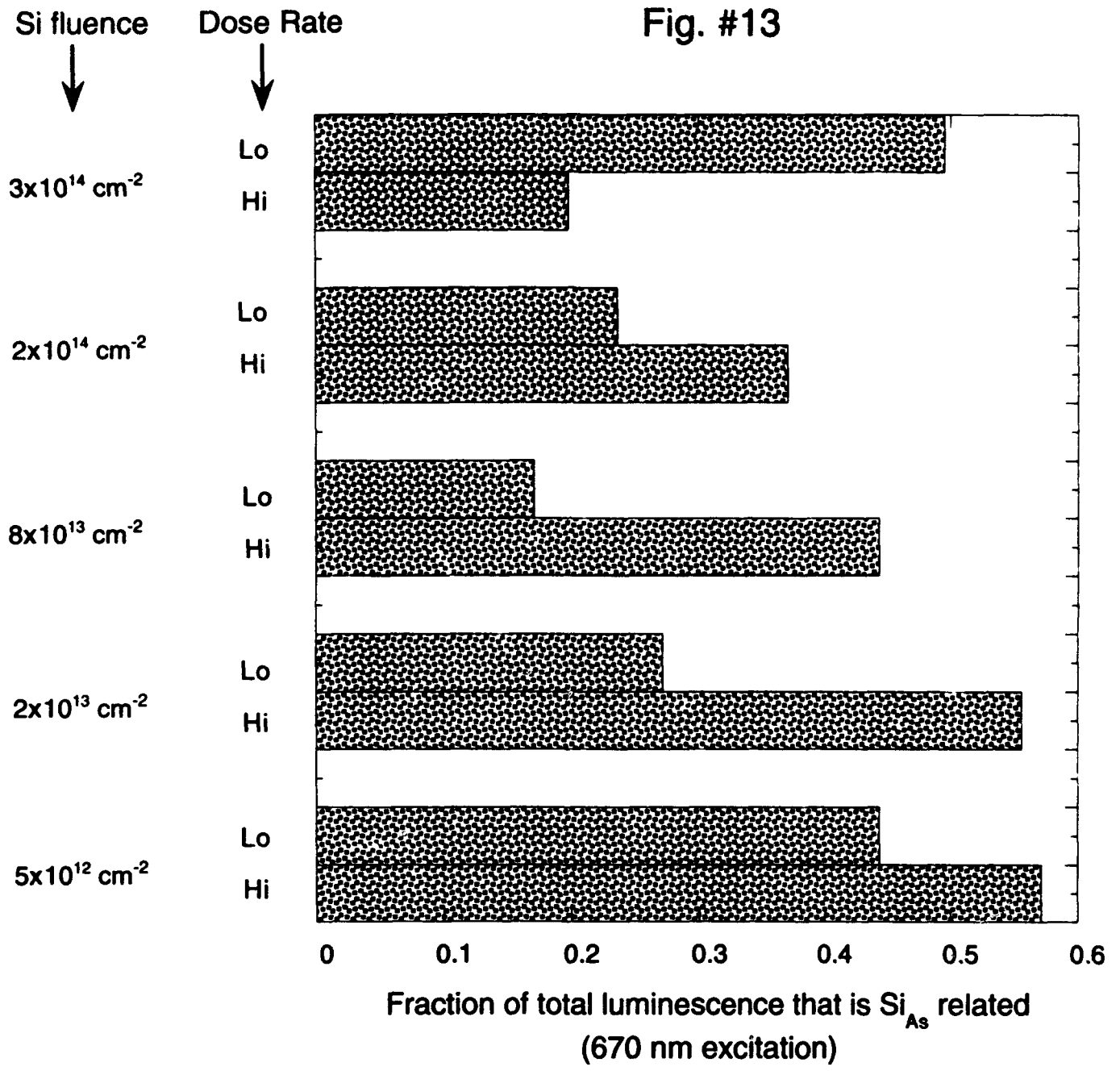


Fig. #14

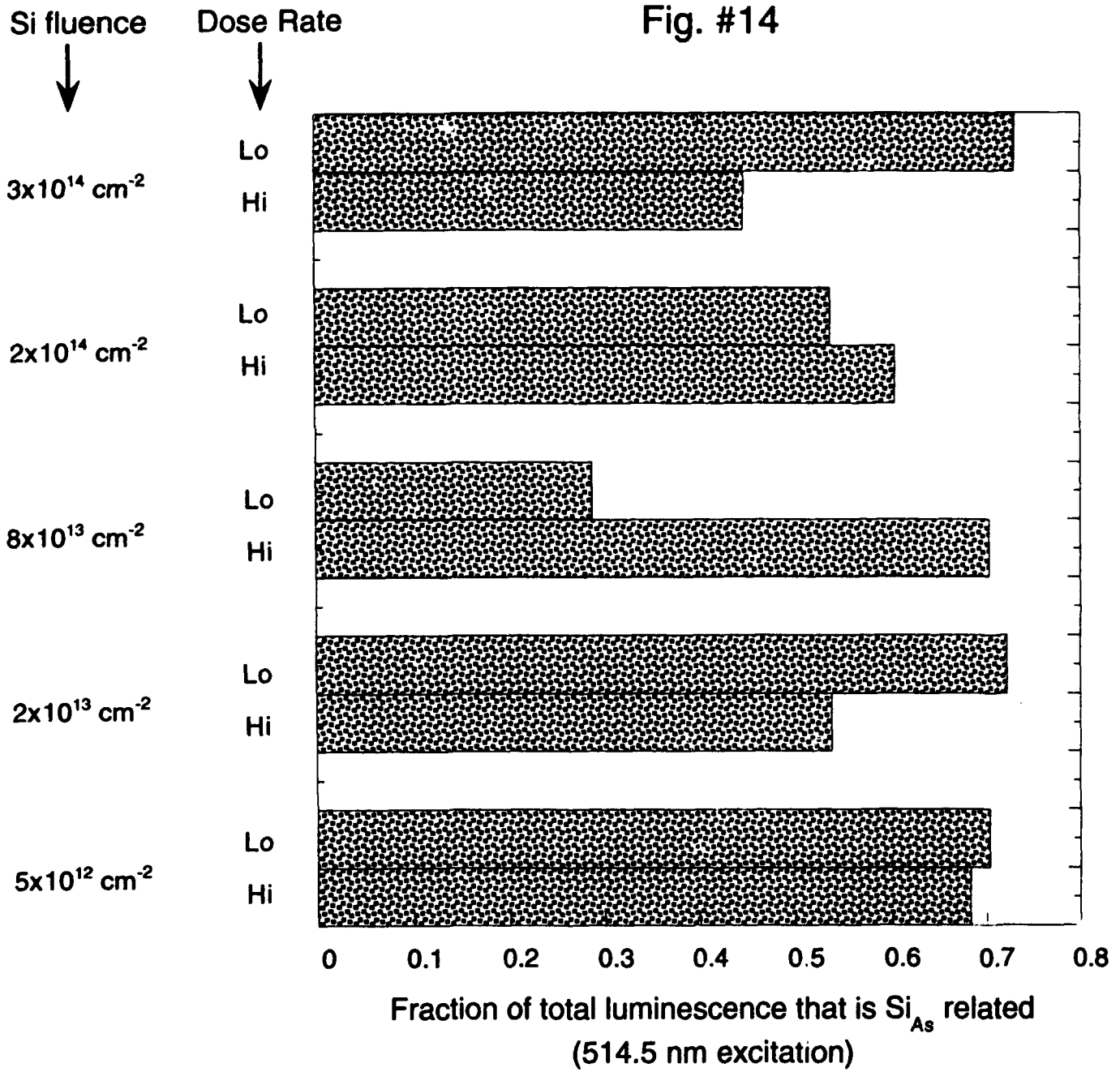


Fig. #15

